RSC Advances

PAPER

View Article Online
View Journal | View Issue

Cite this: *RSC Adv.*, 2017, **7**, 51528

Removal of sulphur from model gasoline by CuAgY zeolite: equilibrium, thermodynamics and kinetics

Yanfei Lu,[a] Rijie Wang,[a] Yue Nan,[b] Fei Liu[a] and Xiaoxia Yang *[a]

In this study, the removal of thiophene from cyclohexane using ion-exchanged Y zeolites was investigated in a batch system by performing static tests. The effects of initial sulphur concentration, contact time and adsorption temperature on the removal efficiency were studied. Changes to the adsorbents before and after the adsorption were characterized by ICP-AES, XRD, N_2 physisorption, SEM, and TEM. The highest sulphur adsorption capacity of 60.98 mgS g^{-1} for CuAgY was achieved at 323 K. The equilibrium data were well fitted by the Sips model and the kinetics of the adsorption process could be described by the pseudo-second-order model. Thermodynamic parameters were obtained from the models and indicated that the adsorption was spontaneous and exothermic. Modeling results also showed that the Marquardt's Percent Standard Deviation (MPSD) and the Sum of the Squares of the Errors (SSE) provided the best fitting results for isotherm and kinetic models, respectively. In addition, it was found that CuAgY could maintain 84.5% of the capacity for sulphur after twice regeneration.

Received 17th October 2017
Accepted 1st November 2017

DOI: 10.1039/c7ra11443e

rsc.li/rsc-advances

1. Introduction

Fuels with high sulphur content could pose a risk to the environment and human health.[1,2] This also inhibits their application to many fields such as fuel cells which require ultra-low sulphur content (less than 0.1 ppmw).[3] Therefore, developing effective deep desulphurization methods is necessary and crucial to satisfy environmental regulations and requirements for ultra-low sulphur fuels.[4–6]

Traditional hydrodesulphurization (HDS) is realized under harsh processing conditions and can effectively remove sulphur compounds including mercaptan and thioether from fuel products.[7] However, it is ineffective in removing thiophene (TP), benzothiophene (BT) and their alkyl derivatives. In order to effectively remove these compounds, a number of new desulphurization technologies have been developed, which include oxidative desulfurization,[8,9] biodesulfurization,[10] extractive desulfurization,[11,12] and adsorptive desulfurization.[13–16] Among these technologies, adsorptive desulphurization was found to be the most promising technique due to its simplicity in system design and low operating cost.

So far, various adsorbents have been studied for adsorption desulphurization such as metal–organic frameworks (MOFs),[17] magnetic alumina,[18] active carbon (AC),[19,20] clay materials,[21] metal oxides,[22] and zeolite-based materials.[13–16,23–33] Y zeolites have been extensively studied due to the large surface area, suitable pore size and thermal stability. The studied Y-based materials included synthesized zeolite ([Ga]AlY),[25] single metal modified zeolites (AgY, Cu(I)Y, NiY, ZnY, CeY, PdY),[26–28] and bimetal modified zeolites ($Cu^{I}Ce^{IV}Y$, AgCeY, CuZnY, NiCeY).[16,29–31]

For single metal modified zeolites, Song *et al.*[14,32] and Yang *et al.*[26,27,33] investigated the removal of thiophenic compounds from transportation fuels (diesel, gasoline and jet fuels) by ion-exchanged Y zeolites with Ag^{+}, Cu^{2+}, Ni^{2+}, Zn^{2+}, Pd^{2+}, and Ce^{3+} cation. The results showed that $Cu^{I}Y$ and AgY zeolites had relatively high sulphur adsorption capacities of 81.6 mgS g^{-1} and 28.8 mgS g^{-1}, respectively, by π-complexation but their adsorption selectivities were adversely impacted by aromatic hydrocarbons. They also found out that $Ce^{IV}Y$ had less impact by aromatic hydrocarbons due to the direct sulphur–metal (S–M) interaction. Among the studies on bimetal modified zeolites, Shan *et al.*[16] found out that the presence of Ce species could enhance the number of Cu^{+} on the $Cu^{I}Ce^{IV}Y$ surface in comparison with $Cu^{I}Y$. The AgCeY, $Cu^{I}Ce^{IV}Y$ and NiCeY had better sulphur adsorption capacity *via* both π-complexation and S–M interaction. In addition, Zhang *et al.*[31] showed that the co-exchanged $Cu^{II}Zn^{II}Y$ was more stable and favorable than AgY in terms of the adsorption desulphurization performance. The co-exchanged $Cu^{II}Zn^{II}Y$ was different to ZnY in terms of desorbing dibenzothiophene in higher temperatures, which may be related with the S–M bonding. Therefore, the bimetal modified Y zeolites have

[a]*Tianjin Key Laboratory of Applied Catalysis Science and Technology, Department of Catalysis Science and Engineering, School of Chemical Engineering and Technology, Tianjin University, Tianjin 300350, People's Republic of China. E-mail: xxy@tju.edu.cn; Fax: +86 2227401018; Tel: +86 2227401018*

[b]*Department of Biomedical and Chemical Engineering, Syracuse University, 329 Link Hall, Syracuse, New York 13244, USA*

a better potential for adsorption desulphurization than single metal modified Y zeolites due to their high capacity and selectivity.

$Cu^{I}Y$ and AgY as π-complexation adsorbents have been developed for adsorption desulphurization. However, they were found not able to meet the requirement of industrial adsorption applications due to some issues. First, they have poor desulphurization performance in real oil samples. Second, after ion exchange, the Cu(II) in CuY has be converted Cu(I) under harsh conditions in order to increase its desulphurization performance which increases the operating cost.[26] Therefore, it would be necessary to develop new bimetallic adsorbents without these drawbacks. Since Cu and Ag exchanged Y zeolites are inexpensive and easy to prepare, this study investigated the adsorption desulphurization performance of CuAgY, which was found to have a high desulfurization capacity.

Besides experimental studies, mathematical model analysis is a practical and efficient way to elaborate the chemical processes and equipment in detail. Song *et al.*[34,35] investigated the model of adsorption kinetics and adsorption equilibrium of TP and BT in model fuel on AgCeY and Cu^{I}-$Ce^{IV}Y$. They found that the Langmuir isotherm and the pseudo-first-order model exhibited the best fits of experimental data, and the intra-particle diffusion was not the rate controlling step. The results were similar to those for NiCeY.[36] Theoretical and empirical models could be used for thermodynamics and kinetics of the adsorption at the solid/liquid interface.

The objective of the current work is to study the removal of TP by adsorption on CuAgY. Its performance was compared with NaY, CuY and AgY. The three factors affecting the adsorption desulphurization performance, the adsorption time, initial sulphur content and temperature, were investigated. The equilibrium, kinetics and thermodynamic systematically properties of adsorption system were studied to understand the adsorption of TP on CuAgY. In addition, the regeneration study of the adsorbents was performed and found that the CuAgY could maintain 84.5% of its capacity after twice regeneration.

2. Experiment

2.1. Materials

Thiophene (Analytical Reagent Grade, 99%), $Cu(NO_3)_2 \cdot 3H_2O$ (99%), and $AgNO_3$ (99.8%) were purchased from Tianjin Guangfu Fine Chemical Research Institute. Cyclohexane (Analytical Reagent Grade, ≥99.7%) was purchased from Tianjin Yuanli Chemical Corporation. All reagents were used without further purification. NaY zeolite ($SiO_2/Al_2O_3 = 4.8$) was purchased from Nankai University Catalyst Factory.

The model gasoline with different sulphur concentrations were prepared by dissolving TP in cyclohexane. The studied sulphur concentrations included: 162 mgS L^{-1} (M-1), 223 mgS L^{-1} (M-2), 305 mgS L^{-1} (M-3), 471 mgS L^{-1} (M-4), 601 mgS L^{-1} (M-5), and 770 mgS L^{-1} (M-6).

2.2. Ion exchange

Prior to the ion exchange, the NaY zeolite was dehydrated in a muffle furnace heating at a rate of 1 K min^{-1} to 673 K and kept at 673 K for 2 h to remove the acid gases, such as CO_2, SO_2 and others. Then NaY zeolite was merged in a 0.1 mol L^{-1} $Cu(NO_3)_2$ or $AgNO_3$ solution at 333 K for 12 h. The ratio of the solution volume (mL) to the mass of NaY (g) was 100 : 1. After the ion exchange was done, the AgY or CuY was filtered and washed thoroughly with deionized water to remove the residual cations. The filtered cake was then dried at 383 K for 6 h and calcinated at 773 K for 4 h. Then the cake was ground into power and stored in a desiccator. The bimetallic zeolites (CuAgY) were prepared by co-exchanging 5 g of NaY in a mixed solution of 250 mL 0.1 mol L^{-1} $AgNO_3$ and 250 mL 0.1 mol L^{-1} $Cu(NO_3)_2$. The procedures were the same as above. The operations with silver nitrate were performed in a dark environment due to the light sensitivity of silver (Table 1).

2.3. Characterization of adsorbents

X-ray powder diffraction (XRD) patterns were obtained with a MinFlex-600 X/Rigaku Diffractometer equipped with Cu Kα radiation ($\lambda = 1.54056$ Å) at 40 kV and 15 mA. The patterns were recorded with the 2θ ranging from 5° to 50° at a scanning rate of 5° min^{-1}. The chemical composition of cation-exchange zeolites was measured by inductively coupled plasma atomic emission spectrometry (ICP-AES) with a Perkin-Elmer Spectrometer. The surface morphologies of the zeolites were characterized by field emission scanning electron microscopy (SEM, Hitachi S-4800). Transmission electron micrographs (TEM) were taken with a Transmission Electron Microscope (JEOL JEM-2100F). N_2 physisorption was measured on a Micromeritics ASAP 2020 (Micromeritics; USA) using nitrogen adsorption at 77 K (Table 2).

Table 1 The three isotherm models evaluated in this study

Isotherms	Equations	
Langmuir[34]	$q_e = \frac{K_L q_m C_e}{1 + K_L C_e}$	(2)
Freundlich[30]	$q_e = K_f C_e^{1/n}$	(3)
Sips[37]	$q_e = \frac{Q(bC_e)^{1/m}}{1 + (bC_e)^{1/m}}$	(4)

Table 2 Kinetic models used in this study

Models	Equations	
Pseudo-first-order	$q_t = q_e(1 - \exp(-k_1 t))$	(8)
Pseudo-second-order	$q_t = \frac{k_2 q_e^2 t}{1 + k_2 q_e t}$	(9)
Intra-particle diffusion	$q_t = kt^{0.5} + C$	(10)

Table 3 Equation of these six different error functions

Error functions	Equations	
SSE	$\sum_{i=1}^{n}(q_{cal}-q_{exp})_i^2$	(11)
HYBRID	$\frac{100}{n-p}\sum_{i=1}^{n}\left[\frac{(q_{cal}-q_{exp})^2}{q_{exp}}\right]_i$	(12)
ARE	$\frac{100}{n}\sum_{i=1}^{n}\left\|\frac{q_{cal}-q_{exp}}{q_{exp}}\right\|_i$	(13)
MPSD	$100\sqrt{\frac{1}{n-p}\sum_{i=1}^{n}\left(\frac{q_{cal}-q_{exp}}{q_{exp}}\right)_i^2}$	(14)
SAE	$\sum_{i=1}^{n}\left\|q_{cal}-q_{exp}\right\|_i$	(15)
R^2	$\frac{\sum(q_{cal}-q_{aexp})^2}{\sum(q_{cal}-q_{aexp})^2+(q_{cal}-q_{exp})^2}$	(16)

2.4. Batch adsorption experiments

For each experiment, 25 mL of model gasoline was mixed with 0.20 g adsorbent in a 100 mL three-necked, round-bottomed flask. The flask was agitated with a magnetic stirrer at a constant speed. A furnace was used to heat the solution to desired temperatures (30, 40, 50 °C). Model gasoline samples were taken during the course of adsorption experiments to obtain kinetic data of the adsorption. After the adsorption was finished, the precipitate was removed by centrifugation and the supernatant was analyzed (Table 3).

2.5. Determination of the sulphur adsorption capacity

The sulphur concentrations of the model gasoline samples taken during the adsorption process were measured using a Gas Chromatograph (GC-6820) equipped with a flame ionization detector (FID). A DB-FFAP column with a length of 60 m and inside diameter 0.32 mm was used. The temperatures of the injector, detector, and oven were set as 200 °C, 250 °C, and 80 °C, respectively.

The amount of sulphur adsorbed at equilibrium (q_e (mgS g^{-1})) was calculated by:

$$q_e = \frac{(C_0 - C_e)V}{m_0} \quad (1)$$

3. Theoretical basis of models

3.1. Adsorption isotherm models

Three different adsorption isotherm models, namely Langmuir, Freundlich, and Sips, were used to analyze the adsorption isotherms.

3.2. Adsorption thermodynamics

For adsorption process, the thermodynamic analysis is a key method to judge whether the adsorption process is spontaneous and exothermic or endothermic. The thermodynamic parameters (ΔG^0, ΔH^0, and ΔS^0) of the studied adsorption system can be evaluated according to the following equations:[38,39]

$$C_s \xrightarrow{\lim} \infty \frac{C_s}{C_e} = K_p \quad (5)$$

$$\Delta G^0 = -RT \ln K_p \quad (6)$$

$$\ln K_p = \frac{-\Delta H^0}{R} \times \frac{1}{T} + \frac{\Delta S^0}{R} \quad (7)$$

where K_p is dimensionless sorption distribution coefficient. The value of K_p is equal to the intercept in the plotting $\ln(C_s/C_e)$ *versus* C_s by extrapolating C_s to zero.[39]

3.3. Kinetic models

To better understand of the adsorption kinetics, models including pseudo-first-order, pseudo-second-order, and intra-particle diffusion models were used to fit the experimental

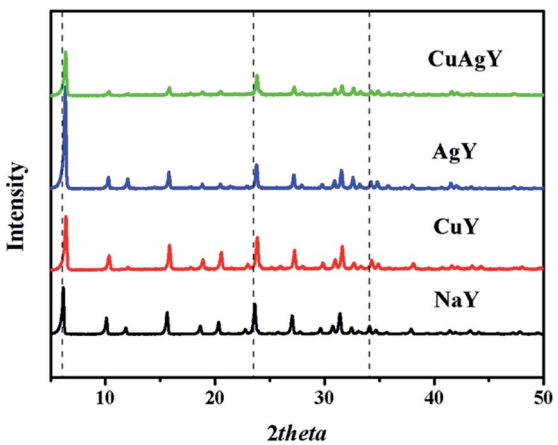

Fig. 1 XRD patterns of NaY, CuY, AgY, and CuAgY.

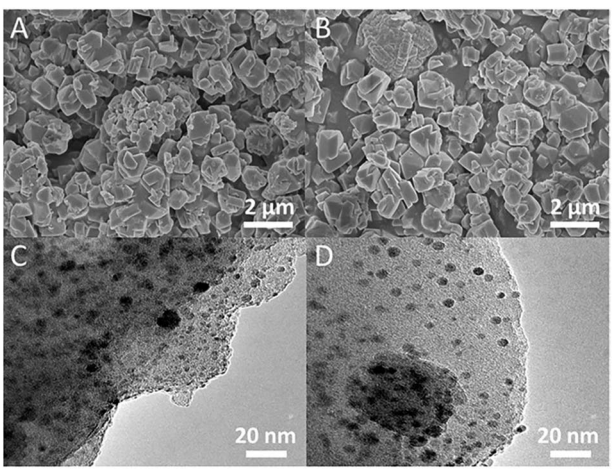

Fig. 2 SEM images (A, C) and TEM images (B, D) of CuAgY before and after TP adsorption.

Table 4 Chemical and physical properties of various zeolites

Zeolites	n(Na)/n(Al)[a]	n(Cu)/n(Al)[a]	n(Ag)/n(Al)[a]	n(Si)/n(Al)[a]	V_{mic}[b] cm^3 g^{-1}	S_{BET}[c] m^2 g^{-1}	S_{mic}[c] m^2 g^{-1}
NaY	0.97	0	0	2.40	0.333	662	626
CuY	0.19	0.40	0	2.42	0.298	604	562
AgY	0.05	0	0.94	2.41	0.319	607	577
CuAgY	0.02	0.26	0.47	2.43	0.295	591	554

[a] Measured by ICP. [b] BET method. [c] t-plot method.

data. These models have been widely used to describe the kinetics of sulphur adsorption on zeolites.[34–36]

3.4. Error functions

The modelling optimization requires error functions to determine the goodness of the fitting by the models. In addition to the correlation coefficients (R^2), five different error functions including the Sum of the Squares of the Errors (SSE), the Hybrid Fractional Error Function (HYBRID),[41] the Average Relative Error Function (ARE), the Marquardt's Percent Standard Deviation (MPSD),[42] and the sum of the Absolute Errors Function (SAE) were used to evaluate the models.[40] The model parameters were evaluated by the solver add-in with Microsoft Excel by minimizing the Sum of Normalized Errors (SNE)[43,44] of the curve-fitting.

4. Results and discussion

4.1. Chemical and physical properties of various zeolites

XRD analysis was used for identifying changes to the mineralogical structures of the zeolites after modifications. The results in Fig. 1 showed that all the characteristic peaks of the modified NaY closely matched with those in original NaY. No additional phases/peaks were observed. Therefore the crystal structure of modified zeolites maintained the same. However, the crystallinities of these modified zeolites slightly decreased due to a decrease in the intensity of peaks. Meanwhile, the positions of the peaks for the modified NaY zeolites were slightly shifted to angles higher than those for NaY, which indicated a reduction in the d-spacing value due to the Bragg equation. These

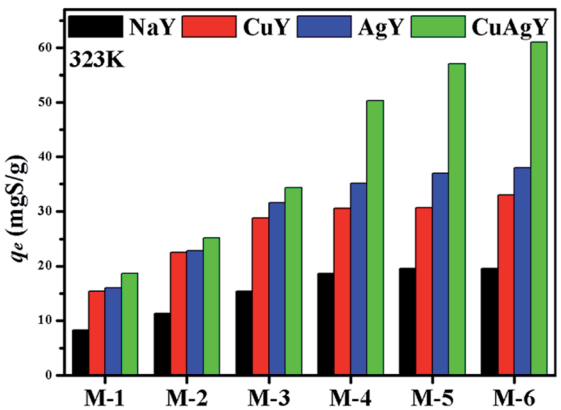

Fig. 3 The adsorption sulphur capacities on NaY, CuY, AgY, and CuAgY at 323 K.

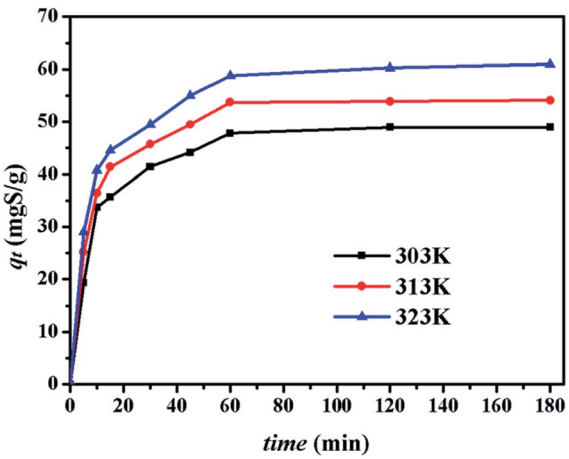

Fig. 4 Effect of contact time on desulphurization on CuAgY at different temperatures.

Table 5 Adsorption capacities of the TP adsorption on various adsorbents

Adsorbents	Adsorbate/solvent	C_0 (mg L^{-1})	Adsorption mode	q_e (mgS g^{-1})	Ref.
HYD10B-MS-13X	TP/n-hexane	707	Batch	4.78	47
Ni/SBA	TP/n-octane	407	Fix bed	7.04	48
MnO/AC	TP/(n-hexane and toluene)	36	Batch/fix bed	1.58	49
Nickel NPs	TP/n-octane	524	Batch	25.0	50
HKUST-1/Fe_3O_4	TP/isooctane	450	Batch	19.8	51
AgCeY	TP/n-octane	100	Batch	1.70	34
$Cu^{I}Ce^{IV}Y$	TP/isooctane	381	Batch	38.4	16
NiCeY	TP/n-octane	703	Batch	22.4	36
CuZnY	TP/n-octane	351	Batch	17.2	31
CuAgY	TP/cyclohexane	778	Batch	60.98	This study

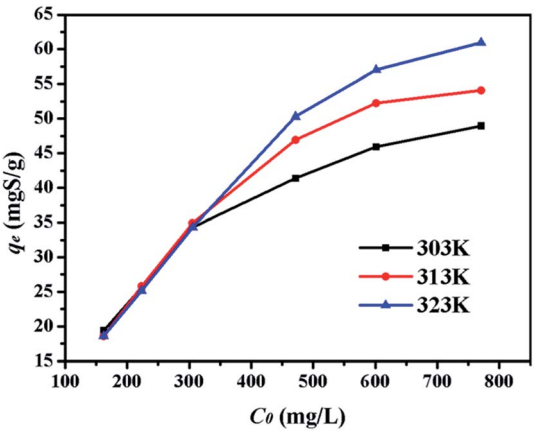

Fig. 5 Effect of C_0 on adsorption capacity of CuAgY at different temperatures.

observations indicated the physical structure of FAU framework was nearly unchanged. Similar results have been provided in other literature.[45] The SEM and TEM images of CuAgY zeolite before and after adsorption were shown in Fig. 2. In general, the SEM and TEM image of CuAgY showed the presence of crystals with the irregular cubic shaped structure, smooth and homogenous surface morphology without clusters forming. It indicated that the adsorbent was very stable. Results of nitrogen physisorption to determine the physical properties of original NaY and modified NaY were shown in Table 4. The micropore volume of CuAgY was 0.295 $cm^3\ g^{-1}$, which was lower than that of NaY. It might be related to the partly collapse of zeolite structure. This phenomenon was consistent with the XRD results. ICP-AES was used to obtain the fraction of total silicon, aluminum, and metal ions. The original NaY and modified NaY were shown in Table 4. Since metal cations (M) in the zeolites balanced the negative charge of the aluminum tetrahedron, the $n(mM^{m+} + Na^+)/n(Al)$ ratio should be 1 : 1 due to the law of conservation of charge. As shown in Table 4, the ratios of $n(2Cu^{2+} + Na^+)/n(Al)$, $n(Ag^+ + Na^+)/n(Al)$, and $n(2Cu^{2+} + Ag^+ + Na^+)/n(Al)$ are all close to 1. However, the $n(Si)/n(Al)$ ratio increases after preparation. It indicates that the minority of framework aluminum dissolves in ion exchange and high-temperature calcination results in the collapse of zeolite structure.

Table 6 SNE and error analysis for Langmuir, Freundlich, and Sips at 303 K

	SSE	HYBRID	ARE	MPSD	SAE
Langmuir					
q_m (mgS g^{-1})	49.33	49.09	49.06	49.06	49.06
K_L (L mg^{-1})	0.0542	0.0552	0.0598	0.0598	0.0598
SSE	16.00	16.11	18.93	18.93	18.93
HYBRID	11.40	11.33	13.85	13.85	13.85
ARE	1.845	1.767	1.042	1.042	1.042
MPSD	13.13	13.15	11.46	11.46	11.46
SAE	8.643	8.804	7.993	7.993	7.993
SNE	4.649	4.627	4.344	**4.344**	4.344
Freundlich					
K_f (mg g^{-1}) (L $mg^{-1})^{1/n}$	13.31	12.42	10.00	11.89	13.31
$1/n$	0.2233	0.2367	0.2769	0.2455	0.2250
SSE	35.94	37.95	67.52	41.25	36.55
HYBRID	32.06	30.15	47.51	30.86	32.62
ARE	3.900	3.181	1.727	2.753	3.947
MPSD	20.15	17.95	19.00	16.59	20.05
SAE	11.57	11.06	13.62	10.72	11.36
SNE	4.045	3.705	4.380	**3.568**	4.057
Sips					
Q (mgS g^{-1})	52.92	52.31	52.70	61.32	52.28
b (L mg^{-1})	0.0462	0.0472	0.0468	0.0252	0.0472
$1/m$	0.780	0.807	0.808	0.599	0.807
SSE	13.14	13.22	13.41	19.93	13.23
HYBRID	12.46	12.35	12.61	19.22	12.35
ARE	1.047	0.950	0.924	0.696	0.950
MPSD	11.92	11.54	11.74	8.74	11.52
SAE	7.149	7.065	7.218	5.349	7.048
SNE	4.299	4.161	4.197	**4.139**	4.158

4.2. Batch adsorption experimental results

4.2.1. Effect of NaY and modified NaY zeolites. The desulphurization performances of the original NaY and modified NaY zeolites were studied, and the results are shown in Fig. 3. It was found that the modified NaY zeolites had higher desulfurization removal, which should be due to π-complexation when Cu or Ag was added.[27] Among the modified NaY zeolites, CuAgY achieved the highest loading of 60.98 mgS g^{-1}. The sulphur capacity of AgY is 32.00 mgS g^{-1}, which was in good agreement with the results reported in the literature.[46] The adsorption sulphur capacity of different adsorbents for removing TP in other literatures are listed in Table 5.

4.2.2. Effect of contact time. The effect of contact time on the adsorption capacity of CuAgY was studied. As shown in Fig. 4, the sulphur adsorption capacity on CuAgY increased at all temperatures and reached the dynamic balance from 60 min

Table 7 Comparison of the Langmuir, Freundlich, and Sips at different temperatures

	303 K	313 K	323 K
Langmuir			
q_m (mgS g^{-1})	49.06	59.80	72.74
K_L (L mg^{-1})	0.0598	0.0338	0.0199
R^2	0.9894	0.9911	0.9852
MPSD	11.46	13.74	13.68
Freundlich			
K_f (mg g^{-1})(L $mg^{-1})^{1/n}$	11.89	9.30	6.68
$1/n$	0.245	0.328	0.399
R^2	0.9779	0.9435	0.9203
MPSD	16.59	33.63	35.09
Sips			
Q (mgS g^{-1})	61.32	54.12	64.76
b (L mg^{-1})	0.0252	0.0410	0.0288
$1/m$	0.5992	1.6435	1.3394
R^2	0.9890	0.9955	0.9978
MPSD	8.74	7.78	7.76

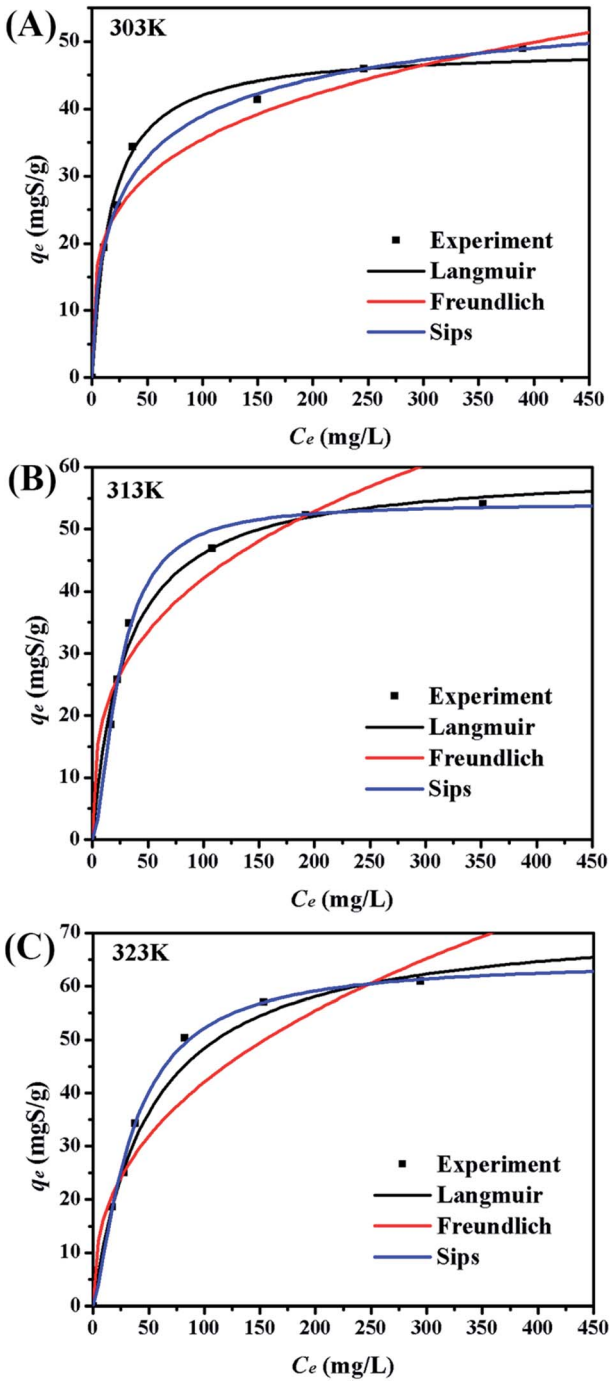

Fig. 6 Adsorption equilibrium isotherms on CuAgY at different temperatures.

to 180 min. Within the first 20 min, the adsorption rate was found to increase with increasing temperature. Increasing the temperature in the beginning was beneficial to heat and mass transfer, and the interaction between adsorbent and adsorbate.

4.2.3. Effect of initial sulphur concentration. Adsorption experiments were executed with different initial sulphur concentrations at 303 K, 313 K, and 323 K to obtain the equilibrium data of sulphur adsorption on CuAgY in Fig. 5. At all temperatures, the adsorption equilibrium increased with initial sulphur concentration due to concentration driving force. At 313 K, the sulphur capacity on CuAgY increased from 18.61 mgS g^{-1} to 60.98 mgS g^{-1}.

4.3. Modeling of adsorption isotherms

Five error functions were used to fit the experimental data and SNE was applied to evaluate the best error function for the Langmuir, Freundlich, and Sips models. The model parameters and error functions results are summarised in Table 6. MPSD was accounted as the best error function for estimating the isotherms due to the minimum SNE as highlighted in bold type in Table 6. The lowest SNE using the MPSD function were calculated as 4.344, 3.568, and 4.139 for Langmuir, Freundlich and Sips models, respectively. The modeling results for all three models and temperatures are compared in Table 7. The Sips model has lowest MPSD values and highest R^2, which indicate that the Sips model fits the isotherms of TP adsorption on CuAgY best. The experimental adsorption data were fitted using the three isotherm models, which are shown in Fig. 6.

4.4. Adsorption kinetics

The kinetics of sulphur adsorption on CuAgY was analyzed with three widely used kinetic models for adsorption processes including pseudo-first-order, pseudo-second-order, and intra-particle diffusion models. Similar to the analysis of isotherms above, the five error functions were used and SNE were evaluated to determine the best error function for the pseudo-first-order and pseudo-second-order models. Model parameters and error functions analysis results are given in Table 8. The SNE values in bold shown in Table 8 indicated that the SSE error function was best one for optimizing the kinetics. The parameters estimated for different temperatures using the two kinetics models as well as the SSE and R^2 values are shown in Table 9. It was found that the pseudo-second-order model had the lowest SSE values and R^2 values above 0.99, which indicated that this model fit the uptake curve of sulphur on CuAgY best. Fittings of experimental data with the pseudo-first-order and pseudo-second-order models are demonstrated in Fig. 7 and 8. The rate constant k_2 of the pseudo-second-order model were 0.00286, 0.00301, 0.00271 g mg^{-1} min^{-1} for different temperatures and the model predicted q_e was close to the actual q_{exp}. Hence, the pseudo-second-order kinetic model fitted the data better than the pseudo-first-order model. Furthermore, Fig. 9 shows the fitting of the intra-particle model with the kinetic data. The lines of the intra-particle diffusion model mainly contained three fractions at all temperatures. It was found that this model cannot describe the adsorption kinetics of sulphur of CuAgY. It was observed that the figure lines in the Fig. 9 had three fractions. The first fraction indicated the rapid adsorption of TP molecules on the external surface of CuAgY through the boundary film. The second fraction indicated that TP molecules moved from the external surface to the active intra-particle sites the rate of which was controlled by the intra-particle diffusion resulting in a slower uptake rate. The last fraction was the equilibrium stage there no further adsorption occurred. The dotted lines of the intra-particle diffusion model did not pass

Table 8 SNE and error analysis for the pseudo-first-order and pseudo-second-order kinetic at 303 K

	SSE	HYBRID	ARE	MPSD	SAE
Pseudo-first-order					
q_e (mgS g^{-1})	46.91	46.70	47.96	47.96	47.96
k_1 (min^{-1})	0.1065	0.1083	0.1034	0.1034	0.1034
SSE	39.47	39.66	44.50	44.50	44.50
HYBRID	13.85	13.78	15.86	15.86	15.86
ARE	4.233	4.370	4.038	4.038	4.038
MPSD	14.40	14.87	13.74	13.74	13.74
SAE	15.74	16.17	14.60	14.60	14.60
SNE	**4.671**	4.760	4.751	4.751	4.751
Pseudo-second-order					
q_e (mgS g^{-1})	51.66	52.06	52.12	50.95	50.66
k_2 (g mg^{-1} min^{-1})	0.00286	0.00268	0.00248	0.00285	0.00315
SSE	19.06	19.99	25.95	22.90	21.37
HYBRID	9.744	9.260	10.82	10.35	11.52
ARE	3.408	3.394	3.185	3.325	3.503
MPSD	11.59	11.54	10.83	11.31	11.92
SAE	9.441	9.916	9.829	9.533	9.317
SNE	**4.478**	4.511	4.748	4.640	4.763

Table 9 Comparison of the pseudo-first-order, pseudo-second-order kinetic, and Intra-particle models for sulphur adsorption on CuAgY

	Temperature (K)		
	303	313	323
q_{exp} (mgS g^{-1})	48.95	54.08	60.98
Pseudo-first-order			
q_e (mgS g^{-1})	46.90	51.83	57.34
k_1 (min^{-1})	0.1065	0.1172	0.1177
R^2	0.9819	0.9824	0.9727
SSE	39.47	46.08	88.43
Pseudo-second-order			
q_e (mgS g^{-1})	51.66	56.61	62.73
k_2 (g mg^{-1} min^{-1})	0.00286	0.00301	0.00271
R^2	0.9910	0.9960	0.9956
SSE	19.06	9.99	13.70
Intra-particle diffusion			
C (mgS g^{-1})	16.45	19.47	21.29
k (mg g^{-1} min$^{-0.5}$)	3.213	3.450	3.871

through the origin point, which indicated that the intra-particle diffusion was influenced by the boundary layer diffusion.[28,52]

4.5. Adsorption thermodynamics

Thermodynamic parameters including ΔH^0 and ΔS^0 were obtained from the Van's Hoff plot of ln K_p against $1/T$ shown in Fig. 10 and the calculated parameters are listed in Table 10. The negative values of Gibbs free energy change ($\Delta G^0 < 0$) indicated that the adsorption of sulphur on CuAgY was a spontaneous process. The value of ΔG^0 became more negative with the increasing of temperature indicating that the increase of temperature favored the adsorption. The negative value of ΔH^0

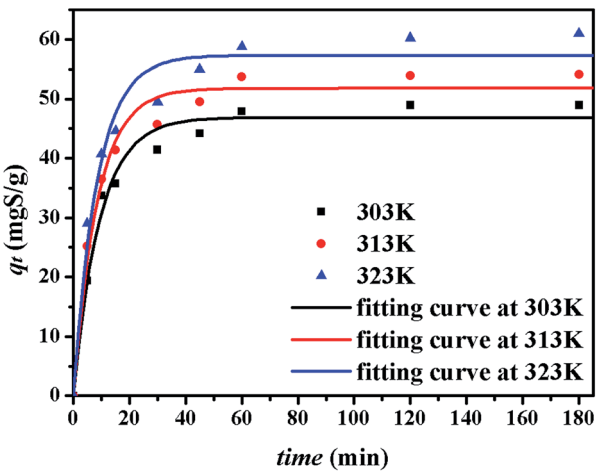

Fig. 7 Uptake curves of sulphur adsorption on CuAgY fitted by the pseudo-first-order model.

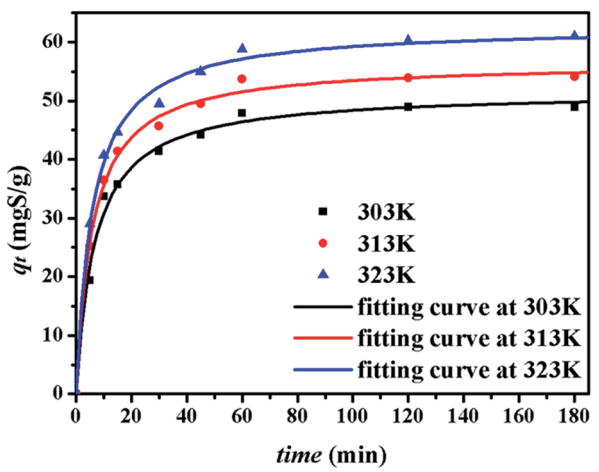

Fig. 8 Uptake curves of sulphur adsorption on CuAgY fitted by the pseudo-second-order model.

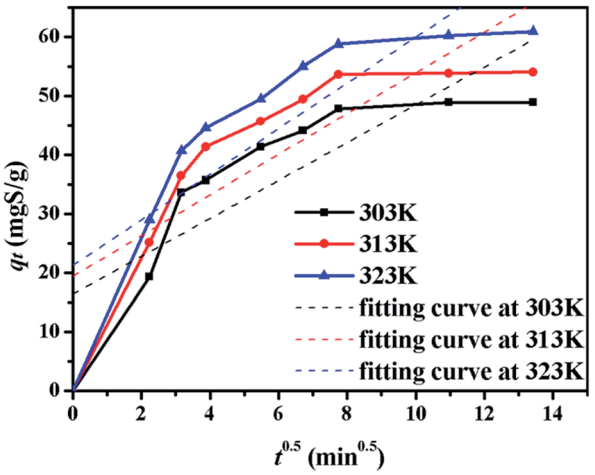

Fig. 9 The plot of q_t *versus* $t^{0.5}$ for sulphur adsorption on CuAgY at different temperatures.

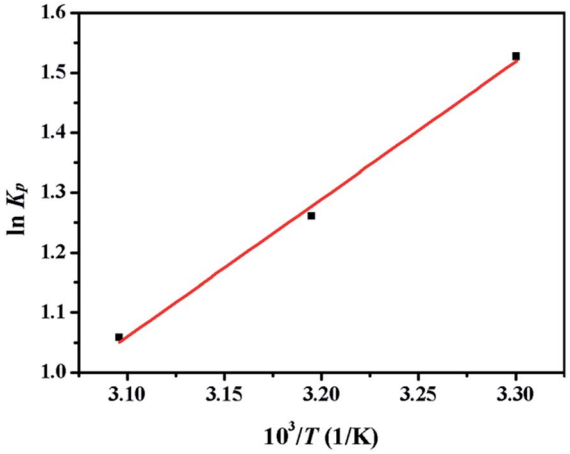

Fig. 10 Plot of ln K_p *vs.* $1/T$ for the estimation of thermodynamic parameters of sulphur adsorption on CuAGY.

manifested that the adsorption was exothermic. The negative entropy ΔS^0 indicated a decrease of randomness at the solid-solution interface during adsorption.

4.6. Regeneration

The used CuY, AgY and CuAgY were regenerated using air-calcination at 633 K for 6 h. The capacities of the regenerated zeolites were evaluated with the M-6. The results shown in Fig. 11 indicated that CuAgY lost 15.5% of capacity for sulphur adsorption in model gasoline after twice regeneration, while CuY and AgY lost about 58.3% and 47.3% of its capacity, respectively. This result showed that CuAgY had better regeneration performance than CuY and AgY.

Table 10 Thermodynamic parameters for adsorption of sulphur on CuAgY

Zeolite	Temperature (K)	K_p	ΔG^0 (kJ mol^{-1})	ΔH^0 (kJ mol^{-1})	ΔS^0 (J K^{-1} mol^{-1})
CuAgY	303	4.61	−3.83		
	313	3.53	−3.32	−19.11	−50.43
	323	2.88	−2.82		

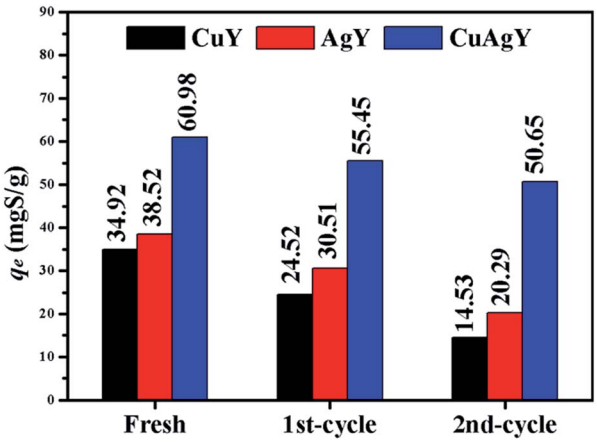

Fig. 11 Regeneration performance of CuY, AgY, and CuAgY for sulphur adsorption.

5. Conclusions

Compared with the adsorption performance on NaY, CuY, and AgY, CuAgY could be regarded as a better alternative, inexpensive, and environmentally benign adsorbent for removing TP. The types of cations and their exchange degree of zeolites were the important factors influencing the adsorption performance. Experimental results indicated that CuAgY had a higher adsorption capacity for sulphur (60.98 mgS g^{-1} at 323 K) than CuY (34.92 mgS g^{-1}) and AgY (38.52 mgS g^{-1}) studied in this work, and most other adsorbents in the literature. The isothermal equilibria could be represented by the Sips model using the MSPD error function and the kinetics of the adsorption process could be described by the pseudo-second-order model with the SSE error function. The negative values of ΔG and ΔH showed that the adsorption was spontaneous and exothermic. After twice regeneration, the sulphur adsorption capacity of CuAgY maintained at 50.65 mgS g^{-1} (15.5% loss), while the CuY and AgY lost 58.3% and 47.3% capacity, respectively, which showed that CuAgY had a good regeneration performance. Further studies are needed to study the effect of the relative content of Cu and Ag on CuAgY on the adsorption performance. As a bimetallic adsorbent, CuAgY with higher sulphur capacity and good regeneration presented a valuable reference for the further research.

Conflicts of interest

There are no conflicts to declare.

Abbreviations

C_0	Initial sulphur concentration (mg L^{-1})
V	Volume of model gasoline (L)
m_0	Mass of adding adsorbent (g)
C_e	Equilibrium concentration of sulphur in model gasoline (mg L^{-1})
C_s	Concentration of adsorbate adsorbed onto the adsorbent at equilibrium (mg L^{-1})
q_e	Uptake of the adsorbate by the adsorbent at equilibrium (mgS g^{-1})
q_m	Maximum capacity (mgS g^{-1})
q_t	Uptake of the adsorbate by the adsorbent at time t (mgS g^{-1})
K_L	Langmuir equilibrium constant (L mg^{-1})
K_f	Freundlich adsorption isotherm constant [(mg g^{-1})(L $mg^{-1})^{1/n}$]
$1/n$	Freundlich constant
Q	Sips characteristic parameters (mgS g^{-1})
b	Sips constant (L mg^{-1})
m	Sips constant
K_p	Sorption distribution coefficient
ΔG^0	Free energy of sorption (kJ mol^{-1})
ΔH^0	Enthalpy changes (kJ mol^{-1})
ΔS^0	Entropy changes (J K^{-1} mol^{-1})
T	Absolute temperature (K)
R	Universal gas constant (8.314 J (mol^{-1} K^{-1}))
k_1	Rate constant of the pseudo-first-order model (min^{-1})
k_2	Rate constant of the pseudo-second-order model (g mg^{-1} min^{-1})
k	Intra-particle diffusion rate constant (mg g^{-1} $min^{-0.5}$)
q_{exp}	Observation from the batch experiment (mgS g^{-1})
q_{cal}	Estimate from the model (mgS g^{-1})
q_{aexp}	Average of q_{exp} (mgS g^{-1})
n	Number of observations in the experimental isotherm
p	Number of constants in models
V_{mic}	Micropore volume (cm^3 g^{-1})
S_{BET}	Total surface area (m^2 g^{-1})
S_{mic}	Micropore surface area (m^2 g^{-1})

References

1 C. Song and X. Ma, *Appl. Catal., B*, 2003, **41**, 207–238.
2 A. Stanislaus, A. Marafi and M. S. Rana, *Catal. Today*, 2010, **153**, 1–68.
3 X. Ma, L. Sun and C. Song, *Catal. Today*, 2002, **77**, 107–116.
4 C. Song, *Catal. Today*, 2003, **86**, 211–263.
5 I. V. Babich and J. A. Moulijn, *Fuel*, 2003, **82**, 607–631.
6 M. Breysse, G. Djega-Mariadassou, S. Pessayre, C. Geantet, M. Vrinat, G. Pérot and M. Lemaire, *Catal. Today*, 2003, **84**, 129–138.
7 M. J. Girgis and B. C. Gates, *Ind. Eng. Chem. Res.*, 1991, **30**, 2021–2058.
8 J. Zhang, A. Wang, X. Li and X. Ma, *J. Catal.*, 2011, **279**, 269–275.
9 J. L. García-Gutiérrez, G. A. Fuentes, M. E. Hernández-Terán, P. García, F. Murrieta-Guevara and F. Jiménez-Cruz, *Appl. Catal., A*, 2008, **334**, 366–373.
10 Y. Izumi, T. Ohshiro, H. Ogino, Y. Hine and M. Shimao, *Appl. Environ. Microbiol.*, 1994, **60**, 223–226.
11 S. Zhang, Q. L. Zhang and Z. C. Zhang, *Ind. Eng. Chem. Res.*, 2014, **43**, 614–622.
12 N. Yi, C. Li, A. Sun, H. Meng and Z. Wang, *Energy Fuels*, 2006, **20**, 2083–2087.
13 X. Ma, A. Michael Sprague and C. Song, *Ind. Eng. Chem. Res.*, 2005, **44**, 5768–5775.
14 X. Ma, S. Velu, J. H. Kim and C. Song, *Appl. Catal., B*, 2005, **56**, 137–147.
15 J. H. Kim, X. Ma, A. Zhou and C. Song, *Catal. Today*, 2006, **111**, 74–83.
16 J. H. Shan, X. Q. Liu, L. B. Sun and R. Cui, *Energy Fuels*, 2008, **22**, 3955–3959.
17 Y. Shi, X. Zhang, L. Wang and G. Liu, *AIChE J.*, 2014, **60**, 2747–2751.
18 G. Shan, H. Liu, J. Xing, G. Zhang and K. Wang, *Ind. Eng. Chem. Res.*, 2004, **43**, 758–761.
19 J. Xiao, C. Song, X. Ma and Z. Li, *Ind. Eng. Chem. Res.*, 2014, **51**, 3436–3443.
20 V. Selvavathi, V. Chidambaram, A. Meenakshisundaram, B. Sairam and B. Sivasankar, *Catal. Today*, 2009, **141**, 99–102.
21 W. Ahmad, I. Ahmad, M. Ishaq and K. Ihsan, *Arabian J. Chem.*, 2014, **50**, 543–549.
22 R. Menzel, D. Iruretagoyena, Y. Wang, S. M. Bawaked, M. Mokhtar, S. A. Al-Thabaiti, S. N. Basahel and M. S. P. Shaffer, *Fuel*, 2016, **181**, 531–536.
23 C. LabordeBoutet, G. Joly, A. Nicolaos, M. Thomas and P. Magnoux, *Ind. Eng. Chem. Res.*, 2006, **45**, 6758–6764.
24 A. J. Hernández-Maldonado and R. T. Yang, *J. Am. Chem. Soc.*, 2004, **126**, 992–993.
25 K. Tang, L. J. Song, L. H. Duan, X. Q. Li, J. Z. Gui and Z. L. Sun, *Sci. China: Chem.*, 2010, **53**, 281–286.
26 A. J. Hernández-Maldonado, F. H. Yang, G. Qi and R. T. Yang, *Appl. Catal., B*, 2005, **56**, 111–126.
27 A. J. H. Hernández-Maldonado and R. T. Yang, *Ind. Eng. Chem. Res.*, 2003, **42**, 123–129.
28 M. Montazerolghaem, A. Rahimi and F. Seyedeyn-Azad, *Chem. Prod. Process Model.*, 2014, **257**, 603–609.
29 H. Song, X. H. Cui, H. L. Song, H. J. Gao and F. Li, *Ind. Eng. Chem. Res.*, 2015, **53**, 14552–14557.
30 J. Wang, F. Xu, W. J. Xie, Z. J. Mei, Q. Z. Zhang, J. Cai and W. M. Cai, *J. Hazard. Mater.*, 2009, **163**, 538–543.
31 Z. Y. Zhang, T. B. Shi, C. Z. Jia, W. J. Ji, Y. Chen and M. Y. He, *Appl. Catal., B*, 2008, **82**, 1–10.
32 S. Velu, X. L. Ma and C. Song, *Ind. Eng. Chem. Res.*, 2003, **42**, 5293–5304.
33 A. J. Hernández-Maldonado and R. T. Yang, *Ind. Eng. Chem. Res.*, 2003, **42**, 3103–3110.
34 H. Song, G. Yang, H. L. Song, X. H. Cui, F. Li and D. D. Yuan, *J. Taiwan Inst. Chem. Eng.*, 2016, **63**, 125–132.
35 H. Song, Y. Chang, W. Xia, M. Dai, H. Song and Z. Jin, *Ind. Eng. Chem. Res.*, 2014, **53**, 5701–5708.

36 L. Fei, J. Rui, R. Wang, Y. Lu and X. Yang, *RSC Adv.*, 2017, **7**, 23011–23020.
37 C. Marínrosas, L. F. Ramírezverduzco, F. R. Murrietaguevara, G. Hernándeztapia and L. M. Rodríguezotal, *Ind. Eng. Chem. Res.*, 2010, **49**, 4372–4376.
38 K. M. Doke and E. M. Khan, *Rev. Environ. Sci. Bio/Technol.*, 2013, **12**, 25–44.
39 J. W. Biggar and M. W. Cheung, *Soil Sci. Soc. Am. J.*, 1973, **37**, 863–868.
40 J. Sreńsceknazzal, U. Narkiewicz, A. W. Morawski, R. J. Wróbel and B. Michalkiewicz, *J. Chem. Eng. Data*, 2015, **60**, 3148–3158.
41 J. F. Porter, G. Mckay and K. H. Choy, *Chem. Eng. Sci.*, 1999, **54**, 5863–5885.
42 D. W. Marquardt, *Jpn. J. Ind. Appl. Math.*, 1963, **11**, 431–441.
43 A. Gunay, *J. Hazard. Mater.*, 2007, **148**, 708–713.
44 Y. S. Ho, J. F. Porter and G. Mckay, *Water, Air, Soil Pollut.*, 2002, **141**, 1–33.
45 M. H. Fan, H. Panezai, J. H. Sun, S. Y. Bai and X. Wu, *J. Phys. Chem. C*, 2014, **118**, 23761–23767.
46 H. Song, W. Xia and X. Sun, *Can. J. Chem. Eng.*, 2013, **91**, 915–923.
47 A. Mohebbi and V. Mohebbi, *Fluid Phase Equilib.*, 2017, **436**, 30–37.
48 S. Aslam, F. Subhan, Z. Yan, Z. Liu, R. Ullah, U. J. Etim and W. Xing, *Chem. Eng. J.*, 2017, **321**, 48–57.
49 T. A. Saleh, K. O. Sulaiman, S. A. Al-Hammadi, H. Dafalla and G. I. Danmaliki, *J. Cleaner Prod.*, 2017, **154**, 401–412.
50 S. Aslam, F. Subhan, Z. Yan, U. J. Etim and J. Zeng, *Chem. Eng. J.*, 2017, **315**, 469–480.
51 T. Peng, X. Y. Xie, X. Q. Liu, T. Pan, G. Chen, P. F. Chen, J. Y. Zhou, Y. Pan and L. B. Sun, *J. Hazard. Mater.*, 2017, **321**, 344–352.
52 E. Salehi, S. S. Madaeni and F. Heidary, *Sep. Purif. Technol.*, 2012, **94**, 1–8.